

## Bright organic long persistent luminescence in difluoroboron $\beta$ -Diketonate systems

Biao Xu<sup>a,b</sup>, Guangming Wang<sup>b</sup>, Hongxin Gao<sup>b</sup>, Tengyue Wang<sup>b</sup>, Zi Ye<sup>b</sup>, Wen Xia<sup>b</sup>, Qianhui Chong<sup>b</sup>, Qianqian Yan<sup>b,\*</sup>, Kaka Zhang<sup>a,b,\*</sup>

<sup>a</sup> College of Chemistry and Materials Science, Sichuan Normal University, Chengdu 610068, China

<sup>b</sup> State Key Laboratory of Organometallic Chemistry and Shanghai Hongkong Joint Laboratory in Chemical Synthesis, Key Laboratory of Synthetic and Self-Assembly Chemistry for Organic Functional Molecules, Ningbo Zhongke Creation Center of New Materials, Shanghai Institute of Organic Chemistry, University of Chinese Academy of Sciences, Chinese Academy of Sciences, 345 Lingling Road, Shanghai 200032, People's Republic of China



### ARTICLE INFO

#### Keywords:

Organic long persistent luminescence  
Difluoroboron  $\beta$ -diketonate  
Phenyl 4-methoxybenzoate  
Dopant-matrix  
Afterglow

### ABSTRACT

Organic room-temperature phosphorescence (RTP) and afterglow materials show great potential for applications in anti-counterfeiting, data encryption, and bioimaging. Among these, the organic long persistent luminescence (OLPL) materials have attracted considerable attention over the past decades. Herein, we present a three-component system with intriguing photophysical mechanism to achieve bright OLPL materials. Difluoroboron  $\beta$ -diketonate ( $\text{BF}_2\text{bdk}$ ) molecules with intramolecular charge-transfer (ICT) character were employed as luminescent dopants. An electron donor, N,N,N',N'-tetramethylbenzidine (TMB), is introduced as a hole-trapping agent, facilitating charge separation and enabling hour-long OLPL emission. Through systematic screening of organic matrices, phenyl 4-methoxybenzoate (MeOPhB) was identified as the optimal matrix to prepare OLPL materials. The resulting  $\text{BF}_2\text{bdk}$ -MeOPhB-TMB systems achieve bright and long-lasting afterglow emission lasting up to 2.5 h under ambient conditions, comparable to the performance of inorganic  $\text{Sr}_2\text{Al}_{14}\text{O}_{25}/\text{Eu}^{2+}$ ,  $\text{Dy}^{3+}$  materials. This offers a versatile framework for extending the design principles of OLPL systems, greatly enriching the repertoire of OLPL materials. Moreover, the aqueous dispersion of this three-component system retains its long-lived afterglow properties, further demonstrating its potential for applications in bioimaging.

### 1. Introduction

Organic room-temperature phosphorescence (RTP) and afterglow materials are characterized by their long-lived excited states, showing promising applications in anti-counterfeiting, information encryption, lighting, and bioimaging.<sup>[1–8]</sup> Among these, organic long persistent luminescence (OLPL) materials have garnered significant attention.<sup>[2,9–14]</sup> Recent advancements have enabled OLPL materials to achieve afterglow durations extending to the hour scale by leveraging retarded charge recombination processes. Compared to inorganic LPL materials, OLPL materials offer numerous advantages. They exhibit excellent flexibility and processability, are free of rare earth elements, and benefit from low production costs and mild synthesis conditions (not exceeding 300 °C). Moreover, their design versatility allows for tunable doping components and adjustable proportions, further enhancing their appeal for diverse applications.

Recent studies have explored donor–acceptor (D–A) based OLPL

systems, where photoexcitation induces intermolecular charge transfer to form exciplexes. These systems undergo charge separation followed by delayed charge recombination. For instance, by doping the donor N, N,N',N'-tetramethylbenzidine (TMB) into the acceptor 2,8-bis(diphenylphosphoryl)dibenzothiophene (PPT), the materials exhibit hour-level OLPL emission under a nitrogen atmosphere after weak or normal excitation.<sup>[2]</sup> The systems can also exhibit OLPL even above 100 °C. However, oxygen quenching significantly degrades their afterglow performance in air. To address this, the same research group proposed a p-type OLPL system in which holes diffuse within a donor matrix until recombining with free radical anions of the acceptor. Incorporating hole-trapping components further extended the emission lifetime ( $\tau$ ) and enhanced oxygen stability, enabling OLPL to persist under ambient conditions.<sup>[12]</sup> Notably, D–A systems of phenothiazine derivatives and their dioxide analogs achieve 25-minute aqueous-phase afterglow through crystalline matrix stabilization of reactive intermediates, enabling high-contrast bioimaging and biosensing applications.<sup>[15]</sup>

\* Corresponding authors.

E-mail addresses: [yanqianqian@sioc.ac.cn](mailto:yanqianqian@sioc.ac.cn) (Q. Yan), [zhangkaka@sioc.ac.cn](mailto:zhangkaka@sioc.ac.cn) (K. Zhang).

Additionally, polymer-based OLPL systems exhibits excellent processability and flexibility.[16] A red afterglow lasting several hours was discovered in a pyrylium salt-induced photopolymerization system, further demonstrating the versatility and potential of OLPL materials for advanced technological applications.[17].

Compared to D-A systems, two-photon ionization (TPI)-triggered OLPL remains less explored. TPI occurs through sequential two-photon absorption, where an excited state is generated upon absorption of the first photon and the second photon promotes it to an ionized state, followed by a retarded charge recombination process. For example, TMB-doped rigid polymer matrices stabilize TMB radical cations, enabling OLPL at 20 K.[18] Moreover, thermally activated delayed fluorescence (TADF) molecules doped in polymethyl methacrylate (PMMA) have been reported to exhibit TPI-triggered OLPL.[19] Additionally, it is reported that triphenylamine (TPA) derivatives possessing charge transfer (CT) property doped into dibenzo[*b,d*]thiophen-2-ylidiphenyl phosphine oxide (DBTSPO) forms films exhibiting stable white TPI-triggered OLPL at room temperature.[20] A series of arylphosphonium salt molecules featuring a D-A architecture was designed, achieving single-component OLPL system triggered by TPI.[21] These findings highlight the versatility of TPI-based mechanisms in advancing OLPL materials, offering new possibilities for the development of innovative organic luminescent systems.

Previous studies show that OLPL systems based on charge separation of exciplexes typically require well-matched the highest occupied molecular orbital (HOMO) and lowest unoccupied molecular orbital (LUMO) energy levels between donor and acceptor components. In certain D-A systems, the charge separation is closely related to the lowest triplet state ( $T_1$ ) of the exciplex, where  $T_1$  energy level must be higher than the CT state. However, the inherently small oscillator strength of intermolecular charge-transfer processes results in inefficient harvesting of singlet and triplet excitons during charge recombination, leading to low photoluminescence quantum yields (PLQYs). Introducing a third component to modulate charge recombination kinetics represents a crucial strategy for enhancing OLPL performance. For TPI-based OLPL systems, high-energy irradiation is generally required to facilitate charge separation, and some materials demand low temperatures to protect ionized species.[19] In general, organic molecules with long-lived excited states are advantageous for charge separation within these systems. Notably, TADF molecules, capable of simultaneously harvesting both singlet and triplet excitons generated during charge recombination, can significantly improve the efficiency and brightness of OLPL systems.

Current OLPL materials mainly rely on D-A charge transfer or TPI mechanisms as classified by their charge-separation processes (Table S1), both involving the critical steps of charge separation and recombination processes.[12,20,22–27] However, other rational design strategies for OLPL materials remain limited compared to the extensively studied RTP systems, with fewer than 40 cases reported to date. In conventional RTP and afterglow systems, high-performance luminescent materials have been widely developed using approaches such as crystallization engineering, molecular aggregation states control, and supramolecular self-assembly, resulting in numerous examples.[28–49] If strategies can be devised to facilitate charge-separated states within RTP systems, it would significantly diversity OLPL materials and enhance their performance for broader applications.

In recent years, the two-component dopant-matrix strategy has been employed by our group and others to develop high-performance organic RTP and afterglow materials. This approach enables flexible component selection, simple synthesis, and cost-effectiveness.[40,46,50–55] Among these systems, difluoroboron  $\beta$ -diketonate ( $\text{BF}_2\text{bdk}$ ) compounds with intrinsic intramolecular charge-transfer (ICT) properties combine excellent RTP performance with synthetic accessibility and structural tunability.[56–62] They possess a relatively small singlet-triplet energy gap ( $\Delta E_{\text{ST}}$ , compared to localized excitation system), which facilitates efficient intersystem crossing (ISC). As an ideal matrix, crystalline

organic small molecules, such as phenyl benzoate (PhB), provide multiple benefits. First, it provides a rigid microenvironment for the luminescent molecules that effectively suppresses nonradiative decay and oxygen quenching. Second, PhB features a high  $T_1$  energy level, thereby preventing triplet-triplet energy transfer from the luminophores to the matrix. Additionally, its substantial dipole moment allows for dipole-dipole interactions with the luminophores, further reducing  $\Delta E_{\text{ST}}$ . In previous reports, the  $\text{BF}_2\text{bdk}$ -PhB systems typically yield RTP or TADF afterglow with afterglow durations on the order of seconds.

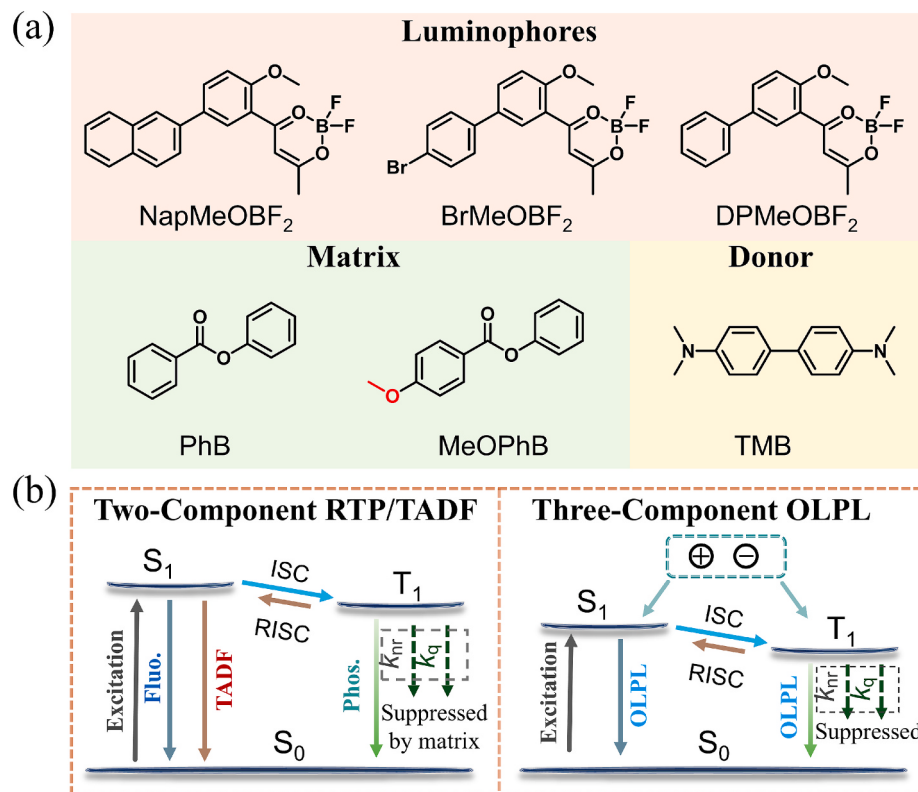
To achieve hour-scale OLPL under weak excitation, we propose introducing an electron donor as a third component into the  $\text{BF}_2\text{bdk}$ -matrix system to construct OLPL materials. The electron donor can engage in charge exchange with the excited states of  $\text{BF}_2\text{bdk}$  molecules, generating charge-separated states. If the electron donor can form a hole trap upon losing an electron, thereby mitigating quenching in the charge-separated state, subsequently, electron-hole recombination would occur at the position of  $\text{BF}_2\text{bdk}$ , facilitating the formation of OLPL, enabling prolonged afterglow lifetimes.

Based on the above ideas, here, we selected the well-established  $\text{BF}_2\text{bdk}$ -matrix two-component system to fabricate long-lived afterglow materials. The third component, TMB, is introduced to the system acting as a hole trap to promote charge separation. We synthesized three  $\text{BF}_2\text{bdk}$  derivatives—NapMeOBF<sub>2</sub>, BrMeOBF<sub>2</sub>, and DPMeOBF<sub>2</sub>—as luminescent molecules and subsequently doped them into PhB matrix or its derivatives. After addition of TMB, the resulting three-component systems of  $\text{BF}_2\text{bdk}$ -matrix-TMB exhibit OLPL properties. Through matrix screening, phenyl 4-methoxybenzoate (MeOPhB) emerged as the optimal choice, demonstrating superior afterglow performance. MeOPhB offers strong dispersion capability for luminophores and the ability to accept electrons to form radical anions. It possesses a significant dipole moment at ground state (2.519 D by DFT calculation). Additionally, its mediate melting point (73.7 °C) facilitates easy processing. Notably, increasing the doping concentration of luminophores in MeOPhB from 0.2 wt% to 0.5 wt% significantly enhanced the brightness of OLPL, achieving an afterglow duration exceeding 2.5 h, comparable to that of inorganic  $\text{Sr}_2\text{Al}_{14}\text{O}_{25}/\text{Eu}^{2+}$ ,  $\text{Dy}^{3+}$  materials. Moreover, aqueous dispersion of these systems also exhibited long-lasting afterglow properties, highlighting their potential for applications in bioimaging and other related fields.

## 2. Results and Discussion

### Synthesis and photophysical properties of $\text{BF}_2\text{bdk}$ .

Using simple aromatic substrates, acetic anhydride, and boron trifluoride etherate as raw materials, three  $\text{BF}_2\text{bdk}$  luminescent molecules—NapMeOBF<sub>2</sub>, BrMeOBF<sub>2</sub>, and DPMeOBF<sub>2</sub>—were synthesized via a one-pot method developed by our group (Scheme 1).[50,51] This method involves a continuous sequence of Friedel-Crafts reaction,  $\beta$ -diketone formation, and boron(III) coordination. The molecular structures were comprehensively characterized by various techniques, including <sup>1</sup>H NMR, <sup>13</sup>C NMR, <sup>19</sup>F NMR, <sup>11</sup>B NMR, HRMS, and FT-IR spectroscopy (Supporting Information, Fig. S55–S72). The structure of NapMeOBF<sub>2</sub> was further confirmed via X-ray single-crystal structure (CCDC 2417108, Fig. S78). The high purity of the  $\text{BF}_2\text{bdk}$  compounds was validated through HPLC analysis (Fig. S81). The UV-vis absorption spectra of NapMeOBF<sub>2</sub>, BrMeOBF<sub>2</sub>, and DPMeOBF<sub>2</sub> in dichloromethane solutions exhibited absorption peaks spanning 250–450 nm (Fig. S1a–c), while their fluorescence spectra revealed maximum emission wavelengths at 531 nm, 498 nm, and 502 nm, respectively (Fig. S1d–f). The emission spectra recorded in various solvents displayed redshifts with increasing solvent polarity, indicating the presence of ICT characteristics (Fig. S1). The photophysical properties were summarized in Table S2. The electron-hole map revealed that the  $\text{BF}_2\text{bdk}$  molecules exhibit ICT features from the electron-rich aromatic functional groups to the electron-deficient dioxaborine moiety, aligning well with the experimental observations (Fig. S2–S4). Furthermore, time-dependent



**Scheme 1.** (a) Chemical structures of NapMeOB<sub>2</sub>, BrMeOB<sub>2</sub>, DPMeOB<sub>2</sub>, PhB, MeOPhB and TMB compounds. (b) Proposed RTP/TADF mechanisms in two-component systems and OLPL mechanisms in three-component systems.

density functional theory (TD-DFT) calculations suggested that the excited states of the luminescent molecules differ significantly between singlet and triplet levels (Fig. S2-S4). According to the El-Sayed rule, this disparity enhances intersystem crossing (ISC). The relatively large spin-orbit coupling matrix element (SOCME) values between the S<sub>1</sub> and T<sub>n</sub> states (around 0.5 cm<sup>-1</sup>) further facilitate the ISC process.

### 3. Preparation and characterization of OLPL materials

The crystalline or powder-state luminescent molecules exhibit no observable afterglow (Fig. S5). When NapMeOB<sub>2</sub> is doped into a PhB matrix at a doping concentration of 0.2 wt%, the resultant melt-cast two-component sample, NapMeOB<sub>2</sub>-PhB-0.2 %, displays a bright afterglow lasting approximately 2 s after excitation with a 365 nm UV lamp (155 mW/cm<sup>2</sup>, Fig. 1a). Similarly, the two-component samples BrMeOB<sub>2</sub>-

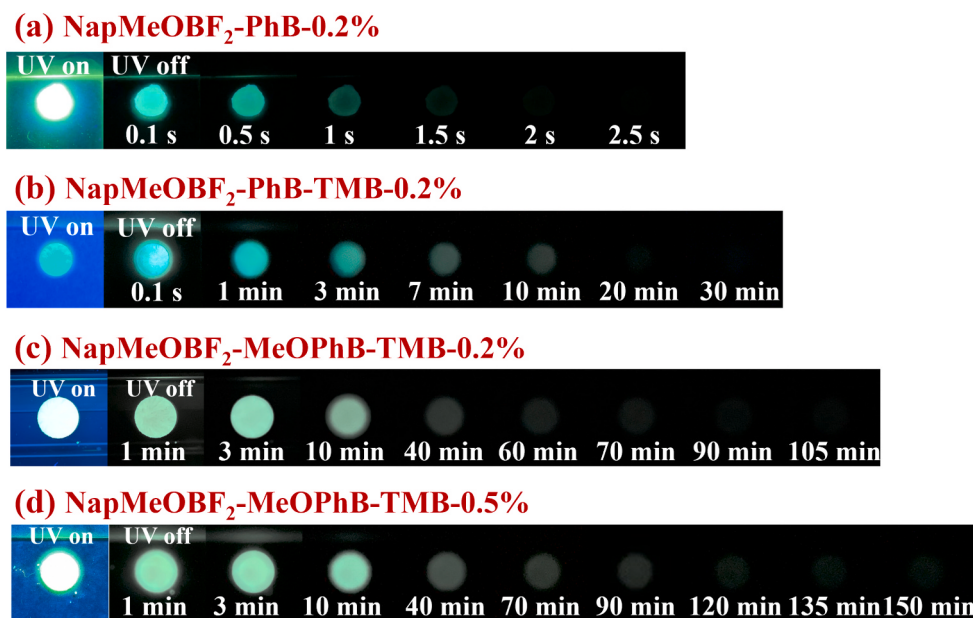


**Fig. 1.** The photographs of (a) NapMeOB<sub>2</sub>-PhB-0.2 %, (b) NapMeOB<sub>2</sub>-PhB-TMB-0.2 %, (c) NapMeOB<sub>2</sub>-MeOPhB-TMB-0.2 % and (d) NapMeOB<sub>2</sub>-MeOPhB-TMB-0.5 % under 365 nm UV light (155 mW/cm<sup>2</sup>) and after ceasing the light source.

PhB-0.2 % and DPMeOBF<sub>2</sub>-PhB-0.2 % also exhibit afterglows of around 2 ~ 3 s under ambient conditions (**Fig. S6**). These can be attributed to the following two aspects. (1) Our previous studies on BF<sub>2</sub>bdk-matrix systems revealed that organic matrices (e.g., PhB and benzophenone with carbonyl functional groups) with relatively large dipole moments can interact with the singlet excited states of BF<sub>2</sub>bdk via dipole–dipole interactions, lower the S<sub>1</sub> energy levels with T<sub>1</sub> levels being less influenced, thereby reducing the singlet–triplet energy gap ( $\Delta E_{ST}$ ) and promoting ISC process, leading to the significant population of triplet excited states.<sup>[50,51]</sup> (2) Molecular aggregation was observed from packing of single-crystal structures of BF<sub>2</sub>bdk (**Fig. S79**), which would cause afterglow quenching. Thus, room-temperature organic afterglow is absent in pure BF<sub>2</sub>bdk samples at room temperature. These findings suggest that the crystalline PhB matrix provides a rigid microenvironment for the luminescent molecules, effectively suppressing their non-radiative decay (**Scheme 1b**). To develop hour-long afterglow materials, a third component, TMB, was introduced (**Scheme 1a**). The three-component system, BF<sub>2</sub>bdk-PhB-TMB-0.2 %, was fabricated via a melt-casting method, with both BF<sub>2</sub>bdk and TMB doped at concentrations of 0.2 wt%. Similar to the BF<sub>2</sub>bdk-PhB-0.2 % samples, the BF<sub>2</sub>bdk-PhB-TMB-0.2 % materials exhibit intense emission upon 365 nm UV light irradiation and bright afterglow after ceasing the light source (**Fig. 1b** and **Fig. S7**). Interestingly, their afterglow duration extended to 30 ~ 50 min compared to BF<sub>2</sub>bdk-PhB-0.2 %. It suggests that the addition of TMB promotes the generation of OLPL. While the afterglow brightness observed in these samples is still relatively weak. Previous studies have underscored the significance of the matrix in designing high-performance afterglow materials, as established in previous studies. To further improve the performance of OLPL materials, many PhB derivatives were designed and synthesized as matrices (**Fig. S8**).

The luminescent molecules NapMeOBF<sub>2</sub>, BrMeOBF<sub>2</sub>, and DPMeOBF<sub>2</sub> were individually doped into these derivative matrices, along with TMB to fabricate three-component samples (BF<sub>2</sub>bdk-matrix-TMB-0.2 %) via a melt-casting method. Initial investigations revealed that BF<sub>2</sub>bdk-MeOPhB-TMB-0.2 %, where BF<sub>2</sub>bdk was doped into the MeOPhB matrix, exhibited superior afterglow performance. Upon excitation with a 365 nm UV lamp, the samples emitted bright cyan-blue emission (**Fig. 1c** and **Fig. S9**). After switching off the UV source, the afterglow durations for NapMeOBF<sub>2</sub>-MeOPhB-TMB-0.2 %, BrMeOBF<sub>2</sub>-MeOPhB-TMB-0.2 %, and DPMeOBF<sub>2</sub>-MeOPhB-TMB-0.2 % reached up to 105 min, 80 min, and 60 min, respectively (**Fig. 1c** and **Fig. S9**), demonstrating the crucial role of matrix in the afterglow system. Interestingly, BrMeOBF<sub>2</sub>-MeOPhB-TMB-0.2 % exhibited enhanced OLPL than DPMeOBF<sub>2</sub>-MeOPhB-TMB-0.2 %, attributed to the heavy-atom effect. While lacking this effect, NapMeOBF<sub>2</sub>-MeOPhB-TMB-0.2 % still showcased remarkable afterglow performance. Notably, compared with BF<sub>2</sub>bdk-PhB-TMB-0.2 %, BF<sub>2</sub>bdk-MeOPhB-TMB-0.2 % displayed significantly enhanced brightness and prolonged afterglow, indicating that the MeOPhB matrix outperformed PhB in the three-component system (**Fig. 1c-d** and **Fig. S7, S9**). Furthermore, concentration variations of NapMeOBF<sub>2</sub> and TMB were explored to optimize the afterglow performance. It was observed that increasing their concentrations from 0.2 wt% to 0.5 wt% resulted in enhanced afterglow brightness (**Fig. 1d** and **Fig. S10**). After being excited by a 365 nm UV lamp, BF<sub>2</sub>bdk-MeOPhB-TMB-0.5 % achieved afterglow brightness and duration comparable to that of inorganic Sr<sub>2</sub>Al<sub>14</sub>O<sub>25</sub>/Eu<sup>2+</sup>, Dy<sup>3+</sup> materials (produced by Obligatory Meteor Jewelry Co., Ltd) activated by sunlight (**Fig. S11**). However, at a doping concentration of 0.6 wt%, a slight reduction in emission intensity was observed, likely due to molecular aggregation (**Fig. S10**). In contrast, for the samples doped in PhB, BF<sub>2</sub>bdk-PhB-TMB samples exhibited diminished afterglow performance at a concentration of 0.5 % (**Fig. S12**), suggesting that the PhB matrix was less effective at mitigating aggregation effects. These findings underline the pivotal role of MeOPhB in effectively dispersing luminescent molecules and enhancing their performance. Additionally, upon excitation with 420 nm visible light, NapMeOBF<sub>2</sub>-MeOPhB-TMB-0.5 % also exhibited bright OLPL (**Fig. S13**).

Based on these results, BF<sub>2</sub>bdk-MeOPhB-TMB-0.5 % materials with promising luminescent performance were selected for further investigation of its photophysical properties.

The steady-state and delayed emission spectra (1 ms delay) of NapMeOBF<sub>2</sub>-MeOPhB-TMB-0.5 % exhibited emission bands in the range of 425–700 nm, with both spectra overlapping and displaying an emission peak at approximately 500 nm (**Fig. 2a**). This observation suggests that the delayed emission probably originates from TADF. Delayed emission spectra recorded at different delayed time confirmed that the signal remained detectable even 1 h after excitation ceased (**Fig. 2b**). The intensity of the delayed emission exhibited a power-law decay as a function of the decay time, described by intensity  $\propto t^{-1.41}$  (**Fig. 2c**). It is consistent with the Debye–Edwards law, where intensity  $\propto t^{-m}$ . Here, the exponent  $m$  represents the charge recombination rate, which typically ranges from 0 to 2.<sup>[63]</sup> A higher  $m$  value indicates a faster decay. The power-law decay of the delayed emission strongly supports an OLPL mechanism (**Fig. S14**). At 77 K, the OLPL intensity decreased sharply, and the  $m$  value dropped to 0.93 (**Fig. S15**), indicating a slower charge recombination rate at low temperatures.

Similarly, the BrMeOBF<sub>2</sub>-MeOPhB-TMB and DPMeOBF<sub>2</sub>-MeOPhB-TMB afterglow materials, where both the doping concentration of BF<sub>2</sub>bdk molecules and TMB are 0.2 wt% or 0.3 wt%, also have been demonstrated OLPL mechanism as the underlying luminescence mechanism (**Fig. S16-S21**, **Table 1**). It should be noted that the delayed emission spectra of BrMeOBF<sub>2</sub>-MeOPhB-TMB and DPMeOBF<sub>2</sub>-MeOPhB-TMB systems deviate from their steady-state spectra (**Fig. S16-S19**). These emission spectra consist of two sets of signals: the one with higher energy is from S<sub>1</sub> states and the other with lower energy is from T<sub>1</sub> states. This assignment is supported by their emission spectra at 77 K (**Fig. S20-S21**). The lower energy signals are unlikely from excimer or molecular aggregate, because most of the emission spectra from BF<sub>2</sub>bdk excimer or molecular aggregate show overall red shift rather than two sets of signals according to our experience on BF<sub>2</sub>bdk systems. We shall note that this assignment doesn't exclude the possibility of BF<sub>2</sub>bdk excimer or molecular aggregate in the system. By comparing the emission spectra of BF<sub>2</sub>bdk-MeOPhB-0.01 % and BF<sub>2</sub>bdk-MeOPhB with higher doping concentrations (*vide infra*), the spectral red shift upon concentration increase can be explained by excimer emission or molecular aggregate formation in the system (**Fig. S26** and **Fig. S30**). Regarding triplet–triplet annihilation (TTA), more experiments were performed on BF<sub>2</sub>bdk-MeOPhB systems, and TTA mechanism has been excluded (*vide infra*).

To further investigate the OLPL properties, we conducted excitation-dependent OLPL measurements (**Fig. S22**). The results demonstrate a clear positive correlation between excitation power and both OLPL intensity and duration. Notably, detectable OLPL signals persist even at excitation power of only 2  $\mu\text{W}/\text{cm}^2$  (**Fig. S22a**), suggesting that the observed OLPL in NapMeOBF<sub>2</sub>-MeOPhB-TMB-0.5 % system is not primarily caused by a TPI mechanism. Furthermore, under a fixed excitation power (2.1 mW/cm<sup>2</sup>), a gradual enhancement in both OLPL intensity and duration with prolonged excitation time was observed (**Fig. S22b**). Significant OLPL afterglow emission was achieved even after excitation of only 5 s, demonstrating the rapid response of these three-component OLPL materials.

#### 4. TADF mechanism of BF<sub>2</sub>bdk luminophores

The bright and persistent OLPL properties observed in the three-component systems are intrinsically related to the TADF characteristics of BF<sub>2</sub>bdk. Consequently, we prepared BF<sub>2</sub>bdk-MeOPhB materials and investigated their photophysical properties. Upon doping NapMeOBF<sub>2</sub> into the MeOPhB matrix at a concentration of 0.5 wt%, the obtained NapMeOBF<sub>2</sub>-MeOPhB-0.5 % exhibited an afterglow duration of approximately 4 s (**Fig. 3a**). Similarly, both BrMeOBF<sub>2</sub>-MeOPhB-0.3 % and DPMeOBF<sub>2</sub>-MeOPhB-0.3 % exhibit bright afterglow with durations recorded at around 1 s and 3 s, respectively (**Fig. S23**).

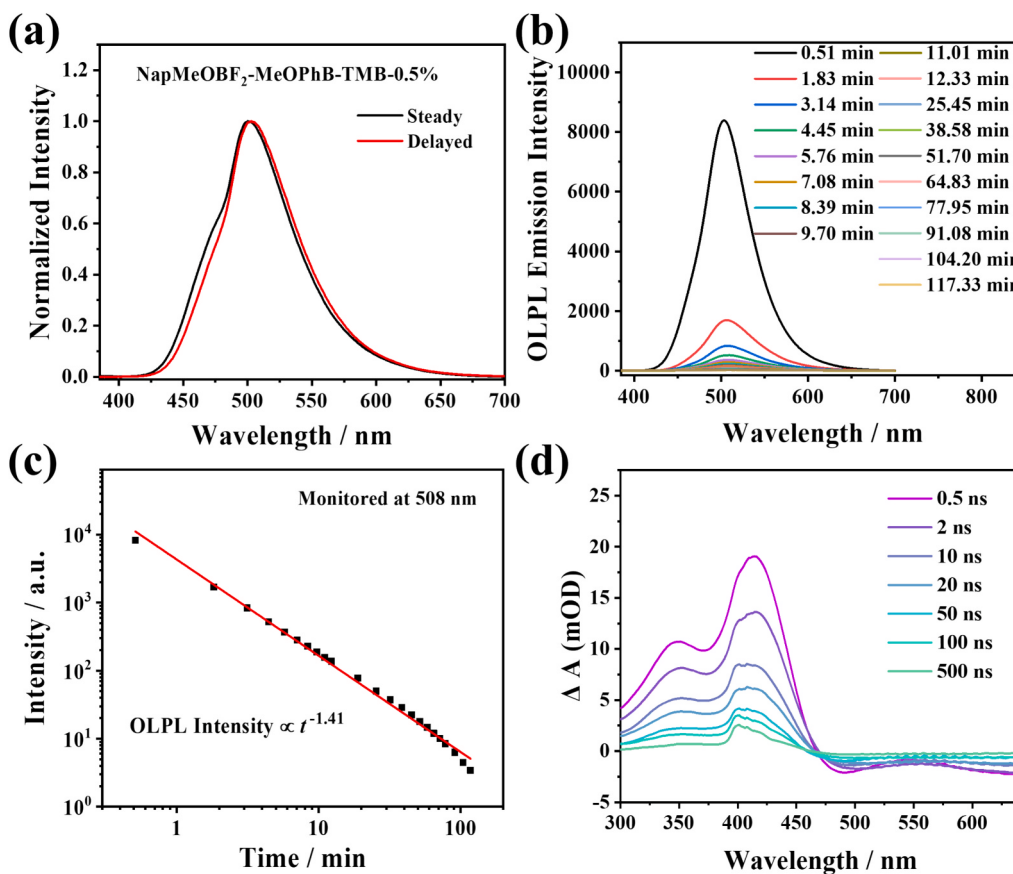


**Fig. 2.** (a) Room-temperature steady-state and delayed emission spectra (1 ms delay) of NapMeOBF<sub>2</sub>-MeOPhB-TMB-0.5 % afterglow materials excited at 365 nm. (b) OLPL emission spectra of the NapMeOBF<sub>2</sub>-MeOPhB-TMB-0.5 % materials excited at 365 nm as a function of delay time. (c) Logarithmic plot of the OLPL emission intensity profile of NapMeOBF<sub>2</sub>-MeOPhB-TMB-0.5 % materials at different delayed time. (d) The transient absorption spectra of NapMeOBF<sub>2</sub>-MeOPhB-TMB-0.5 % sample (excited by a 290 nm pump laser) collected at delay times from 0.5 ns to 500 ns.

**Table 1**  
Photophysical properties of BF<sub>2</sub>bdk-MeOPhB-TMB OLPL materials.

	$\lambda_{\text{Steady}}$ / nm	$\lambda_{\text{Delayed}}$ / nm	$\lambda_{\text{OLPL}}$ / nm	Duration time <sup>a</sup> / s	OLPL intensity <sup>b</sup>	$m$ value	PLQY / %
NapMeOBF <sub>2</sub> -MeOPhB-TMB-0.5 %	500	503	508	>9000	8389	1.41	21.9
NapMeOBF <sub>2</sub> -MeOPhB-TMB-0.2 %	499	500	505	>9000	7482	1.64	/
BrMeOBF <sub>2</sub> -MeOPhB-TMB-0.3 %	472/493	473/494	497	>9000	4229	1.58	19.5
BrMeOBF <sub>2</sub> -MeOPhB-TMB-0.2 %	473	474/490	494	>9000	3756	1.66	/
DPMeOBF <sub>2</sub> -MeOPhB-TMB-0.3 %	474	495	495	>9000	1370	1.40	20.8
DPMeOBF <sub>2</sub> -MeOPhB-TMB-0.2 %	472/491	473/492	473	>9000	1316	1.54	/

<sup>a</sup> Estimated from OLPL emission decay profiles.

<sup>b</sup> Obtained from the OLPL emission spectra at the delay time of 0.51, 0.48, 0.47, 0.45, 0.46 and 0.37 min, respectively.

Both fluorescence and afterglow emission for these samples appeared as bright cyan blue, suggesting that the afterglow may arise from TADF. In the two-component system, the delayed emission spectrum of NapMeOBF<sub>2</sub>-MeOPhB-0.5 % reveals an emission band in the range of 425 to 700 nm, exhibiting identical peak shape and position to the steady-state emission spectrum, with a maximum emission wavelength at 498 nm (Fig. 3b). This observation suggests that the afterglow originates from TADF. The lifetime of excited states followed a double exponential decay with an average lifetime of 47.8 ms (Fig. S24). Temperature-dependent delayed emission of NapMeOBF<sub>2</sub>-MeOPhB-0.5 % sample was studied (Fig. 3c). At 77 K, due to the reverse intersystem crossing ( $k_{\text{RISC}}$ ) is suppressed, only phosphorescent emission was observed with a maximum wavelength at 538 nm and a corresponding lifetime reaching 1317 ms (Fig. S25). With the temperature increasing, TADF at short wavelength is supposed to gradually increase. As a result, the delayed

emission spectra from 223 K to 323 K revealed a blue shift (Fig. 3c). In addition, temperature-dependent measurements of delayed emission lifetimes for the NapMeOBF<sub>2</sub>-MeOPhB-0.5 % materials, monitored at 504 nm, were conducted (Fig. 3d). It was observed that the delayed fluorescence lifetimes decrease as the temperature increases, indicating that the rate of  $k_{\text{RISC}}$  is enhanced with rising temperature (Table S3). From the Arrhenius plot of  $k_{\text{RISC}}$ , the experimental  $\Delta E_{\text{ST}}$  can be estimated to be 0.21 eV (Fig. 3e). It further supports the TADF-type afterglow mechanism proposed in this study. When the doping concentration was reduced to 0.01 wt%, the room-temperature delayed emission spectra of the NapMeOBF<sub>2</sub>-MeOPhB-0.01 % still showed a similar shape and maximum emission wavelength of 494 nm. Therefore, TTA should be insignificant (Fig. S26). For BF<sub>2</sub>bdk-MeOPhB-0.2 %, the power-dependent delayed emission measurements show that the emission intensities show a linear dependence on excitation power density with a

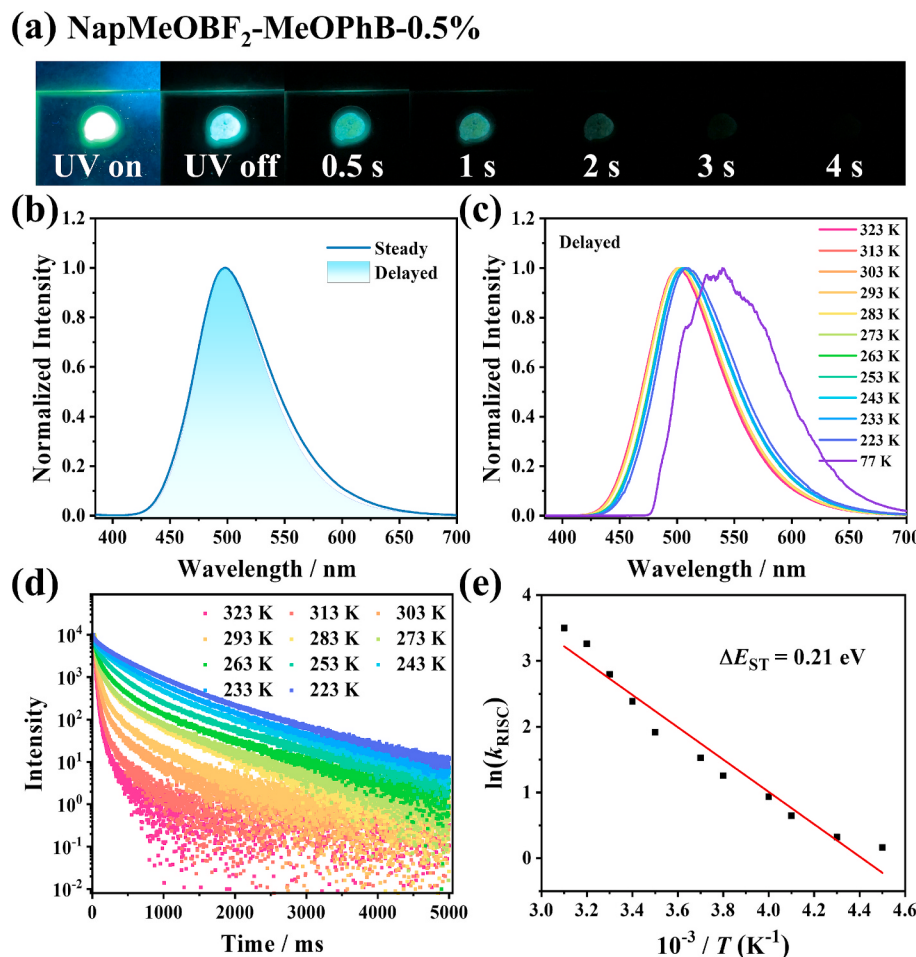


**Fig. 3.** (a) Photographs of NapMeOBF<sub>2</sub>-MeOPhB-0.5 % afterglow materials under 365 nm UV light excitation and after the removal of the UV light. (b) Room-temperature steady-state and delayed emission spectra (1 ms delay) of NapMeOBF<sub>2</sub>-MeOPhB-0.5 % afterglow materials excited at 365 nm. (c) Variable-temperature delayed emission spectra (1 ms delay) of NapMeOBF<sub>2</sub>-MeOPhB-0.5 % materials excited at 365 nm. (d) Temperature-dependent decay profiles of NapMeOBF<sub>2</sub>-MeOPhB-0.5 % materials excited at 365 nm (monitored at 504 nm). (e) Arrhenius plot of  $k_{\text{RISC}}$  from the triplet states to the singlet states of NapMeOBF<sub>2</sub>.

slope value close to 1 in the double-logarithmic plot (Fig. S27). This supports a TADF process, rather than TTA mechanism. High purity of the recrystallization of all components was confirmed via HPLC analysis (Fig. S81), effectively excluding the possibility of impurity-induced afterglow. Furthermore, the  $T_1$  energy level of the MeOPhB matrix significantly exceeds both the  $S_1$  and  $T_1$  levels of NapMeOBF<sub>2</sub> molecules. Such high  $T_1$  levels effectively prevent afterglow quenching via triplet-to-triplet energy transfer from luminescent dopants to the matrices. It has been reported that the excited-state energy transfer from the matrix to dopant can also lead to the emergence of afterglow.[64,65] The MeOPhB matrix exhibits negligible absorption at 420 nm (Fig. S28), while the NapMeOBF<sub>2</sub>-MeOPhB-0.5 % exhibits afterglow emission when excited with 420 nm UV light (Fig. S29). Thereby it is not the case in the present study. These results conclusively demonstrate that the room-temperature afterglow originates from TADF process. For BrMeOBF<sub>2</sub>-MeOPhB-0.3 % and DPMeOBF<sub>2</sub>-MeOPhB-0.3 % samples, their delayed emission spectra overlapping with the steady-state spectra and maximum emission wavelengths around 475 nm (Fig. S30-S33, Table S5). Similar to the three component materials of BrMeOBF<sub>2</sub>-MeOPhB-TMB-0.3 % and DPMeOBF<sub>2</sub>-MeOPhB-TMB-0.3 %, it shows TADF emission with the presence of RTP (*vide supra*). The emission spectra of the samples with a low doping concentration of 0.01 wt% (Fig. S26) and the power-dependent delayed emission measurements of BF<sub>2</sub>bdk-MeOPhB-0.2 % (Fig. S27) exclude the TTA mechanism. The afterglow lifetimes were measured to be 32.7 ms and 159.5 ms, respectively (Fig. S30).

Notably, the PLQYs of NapMeOBF<sub>2</sub>-MeOPhB-0.5 %, BrMeOBF<sub>2</sub>-MeOPhB-0.3 % and DPMeOBF<sub>2</sub>-MeOPhB-0.3 % samples were measured to be 82.0 %, 69.8 %, and 94.3 % by a Hamamatsu absolute PLQY measurement system based on a standard protocol. Upon the introduction of TMB, a significant reduction in PLQY was observed (Table 1). The large difference of PLQY indicates that a significant part of BF<sub>2</sub>bdk excitons participate in the charge separation process, which is the prerequisite for bright OLPL. To estimate the OLPL performance, we find that some reported studies didn't discuss OLPL efficiency because of the lack of technique to directly measure OLPL efficiency, the non-linear dependence of OLPL intensity on excitation power, and other reasons. In view of this, here we propose a relative method to estimate OLPL performance by using a reference. DPMeOBF<sub>2</sub>-PhB-TMB-0.2 % sample can be readily prepared with excellent reproducibility and our group has abundant samples for our study and others.[13] Using this reference, the OLPL performance of other samples can be clearly seen in the OLPL decay profiles (Fig. S34).[13] After integration, the relative OLPL performance of NapMeOBF<sub>2</sub>-MeOPhB-TMB-0.5 % versus DPMeOBF<sub>2</sub>-PhB-TMB-0.2 % can be calculated to be around 6 (Fig. S34).

## 5. Study on OLPL mechanism of BF<sub>2</sub>bdk-MeOPhB-TMB system

Neither BF<sub>2</sub>bdk, MeOPhB, nor TMB exhibits OLPL properties at room temperature in their crystalline or powder states (Fig. S5). The delayed emission spectra of these compounds at 77 K were collected (Fig. S35-40). The delayed emission spectra (1 ms delay) of the BF<sub>2</sub>bdk

compounds in ethyl acetate at 77 K display a distinct band from steady-state spectra, which is derived from phosphorescence emission of the BF<sub>2</sub>bdk compounds. All BF<sub>2</sub>bdk and TMB compounds in ethyl acetate solution and their solid state show no OLPL emission and MeOPhB solid shows very weak emission. The UV-vis spectra of TMB in various solvents display an absorption band at 310 nm (Fig. S41). It shows very weak absorption at 365 nm and negligible absorption at 420 nm. While significant OLPL emission was observed in BF<sub>2</sub>bdk-MeOPhB-TMB system excited by 365 nm or 420 nm light, further demonstrating the excitation of BF<sub>2</sub>bdk is responsible for the photophysical process that ultimately produces OLPL afterglow. The two-component system of BF<sub>2</sub>bdk-MeOPhB shows TADF-type afterglow but no observable hour-long OLPL. As a control, the BF<sub>2</sub>bdk-TMB systems show no afterglow, and the MeOPhB-TMB-0.2 % system exhibits weak OLPL with duration of approximately 4 min after UV excitation (Fig. S42). In the reported studies, the addition of fluorescence dyes into donor-acceptor OLPL systems have been shown to enhance OLPL via excited state energy transfer.<sup>[9,66]</sup> However, upon doping the fluorescent molecules (Fig. S43), such as rubrene or rhodamine B (RhB), into the MeOPhB-TMB-0.2 % system, no enhancement of OLPL can be observed in the resulting three-component materials TMB-MeOPhB-fluorophore-0.2 % (Fig. S44). Therefore, OLPL energy transfer mechanism is not sufficient to explain the drastic enhancement of BF<sub>2</sub>bdk-MeOPhB-TMB's OLPL property. On the other hand, the BF<sub>2</sub>bdk-MeOPhB-TMB system exhibits hour-long OLPL, even when excited by 420 nm visible light (Fig. S13). Given that the MeOPhB-TMB system exhibits minimal absorption at 420 nm, we conclude that the energy transfer from MeOPhB-TMB to BF<sub>2</sub>bdk may occur under UV excitation, but it cannot account for the significant hour-long OLPL, and the visible light excitation characteristics observed in the BF<sub>2</sub>bdk-MeOPhB-TMB system. Reports in the literature described excited-state sensitization of charge separation by TADF molecules, where the OLPL properties of visible-light-excited sensitizer-donor-acceptor systems are comparable to those of UV-excited donor-acceptor systems.<sup>[27]</sup> However, in the present study, the MeOPhB-TMB sample shows only a weak OLPL lasting approximately 4 min upon UV excitation, which is far inferior to the hour-scale OLPL observed in the BF<sub>2</sub>bdk-MeOPhB-TMB material under visible-light excitation. Therefore, the sensitization mechanism discussed in prior

studies cannot account for the high-performance OLPL of our system.

Given that OLPL systems typically involve charge separation and recombination, which generate the radical cation and anion species, transient absorption (TA) spectroscopy was performed on BF<sub>2</sub>bdk-MeOPhB-TMB-0.5 % system (Fig. 2d, Fig. S45). It shows signals in the wavelength ranges of 300–375 nm and 380–460 nm which is attributed to the absorption of MeOPhB radical anions and TMB radical cations, respectively (Fig. 2d). In the reported studies, the absorption band of TMB radical cation ranging from 400 nm to 500 nm can be found from the transient absorption spectra.<sup>[2,67–69]</sup> Therefore, the transient absorption band at 380–460 nm in the present study can be assigned to TMB radical cations. The assignment of the 300–375 nm transient absorption band to MeOPhB radical anions is based on (1) the radical anions of ethyl benzoate exhibit a characteristic absorption band at 310 nm and (2) the extended conjugation in MeOPhB radical anions compared to ethyl benzoate radical anion would induce a red-shifted absorption spectrum, consistent with the observed band shifted to 350 nm. Based on the above experiments and analyses, we propose an OLPL mechanism for BF<sub>2</sub>bdk-MeOPhB-TMB, as illustrated in Fig. 4. Upon photoexcitation, an electron in the HOMO of BF<sub>2</sub>bdk is promoted to its LUMO. The ester group in MeOPhB (LUMO, -1.6 ~ -2.0 eV by DFT), functioning as an electron acceptor, can accept an electron from the LUMO of BF<sub>2</sub>bdk (-2.3 ~ -2.7 eV) to form a radical anion. It should be noted that this process is thermodynamically unfavorable due to the higher LUMO level of MeOPhB. This low thermodynamic favorability accounts for the absence of significant OLPL in the BF<sub>2</sub>bdk-MeOPhB two-component system. In the BF<sub>2</sub>bdk-MeOPhB-TMB system, the TMB donor compensates for this energy mismatch by donating an electron from its HOMO (-4.8 eV) to the HOMO of BF<sub>2</sub>bdk (-6.3 ~ -5.9 eV). This energetically favorable process facilitates effective charge separation, generating TMB radical cations as hole traps and sufficient MeOPhB radical anions. The subsequent slow recombination of these charges at BF<sub>2</sub>bdk molecules leads to the prolonged OLPL observed in the system. It has been reported that TMB radical cation is stable, which is beneficial to reduce nonradiative charge recombination.<sup>[2,70]</sup> Except for TMB, other alternative third components 1 ~ 8 for constructing three component materials were studied (Fig. S46). However, the Nap-MeOBF<sub>2</sub>-MeOPhB-x-0.2 % (x represents compound 1 ~ 8) exhibited

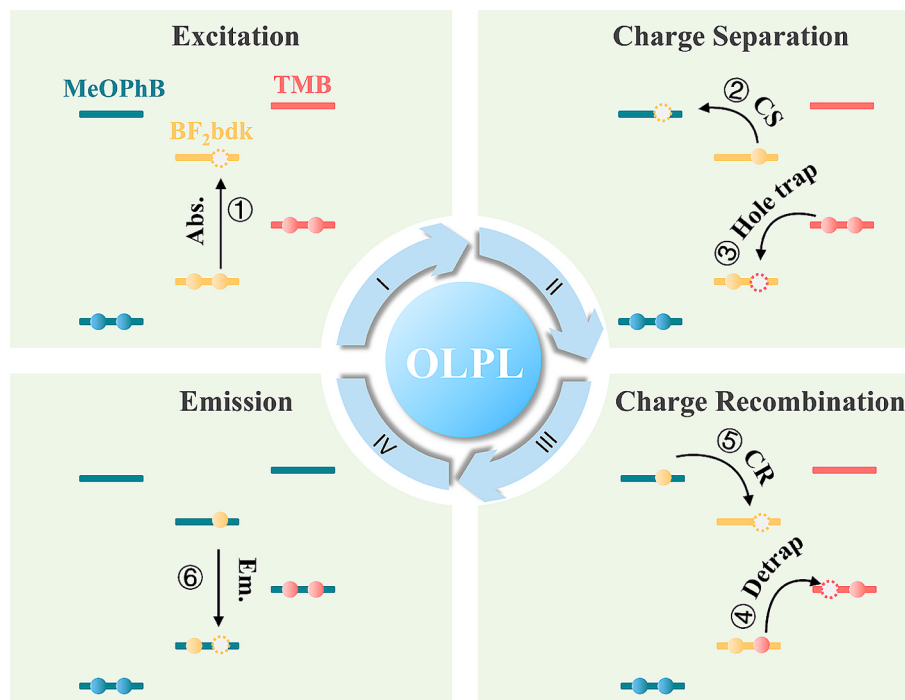


**Fig. 4.** Illustration of BF<sub>2</sub>bdk-MeOPhB-TMB three-component system and the proposed OLPL mechanism.

significantly weaker OLPL performance with an afterglow duration of less than 4 min (Fig. S47). Their steady-state and delayed emission spectra show similar bands with NapMeOB<sub>2</sub>-MeOPhB-TMB-0.2 %, while the OLPL emission is much weaker (Fig. S48-S50).

In the case of the BF<sub>2</sub>bdk-MeOPhB-TMB-0.2 % melt-cast samples, the low doping concentration of compound BF<sub>2</sub>bdk and TMB (0.2 wt%) raises concerns about the feasibility of the proposed electron transfer due to significant spatial separation within the MeOPhB matrix. To validate this electron transfer at a low doping concentration (0.2 wt%), a model experiment was conducted using a classic donor–acceptor pair, tetrathiafulvalene (TTF) and 7,7,8,8-tetracyanoquinodimethane (TCNQ), doped into the MeOPhB matrix at the same low concentration. Interestingly, the resulting TTF-TCNQ-MeOPhB-0.2 % sample exhibited a distinct purple color under daylight, unlike the TTF-MeOPhB-0.2 % and TCNQ-MeOPhB-0.2 % controls (Fig. S37), providing direct evidence that 0.2 wt% doping is sufficient for electron transfer between dopants. This supports the feasibility of electron transfer from TMB to BF<sub>2</sub>bdk in the present three-component system. Additionally, the long-lived excited state characteristics of BF<sub>2</sub>bdk, with an emission lifetime of milliseconds, further enhances the probability of such electron transfer process.

Compared with the examples of OLPL materials in reported studies (Table S1), the present BF<sub>2</sub>bdk-MeOPhB-TMB system exhibits a distinct

charge-separation behavior involving two sequential electron transfers processes that is the electron transfer from LUMO of BF<sub>2</sub>bdk to the LUMO of MeOPhB matrix and the electron transfer from HOMO of TMB to the HOMO of BF<sub>2</sub>bdk. Unlike TPI system, which typically requires high-power excitation, the present BF<sub>2</sub>bdk-MeOPhB-TMB system activates OLPL under normal or low power excitation, with slow charge recombination occurring at BF<sub>2</sub>bdk sites. Furthermore, compared to D-A exciplex systems with relatively small oscillator strength, this system leverages BF<sub>2</sub>bdk's TADF character and high PLQY to efficiently harvest both singlet and triplet excitons generated during charge recombination. Thus, the present BF<sub>2</sub>bdk-MeOPhB-TMB system represents a distinct charge separation mechanism from D-A exciplex and TPI systems but combine the advantages of normal/low-power excitation and efficient charge recombination from both reported systems. In addition, it is cost-effectiveness, as MeOPhB is significantly more affordable than the electronic chemicals such as PPT and 2,2',2''-(1,3,5-benzinetriyl)-tris(1-phenyl-1-H-benzimidazole) (TPBi) commonly employed in the reported OLPL systems.

## 6. Function of materials

Benefiting from the moderate melting point of the matrix, the three-component OLPL materials can be readily processed into diverse shapes

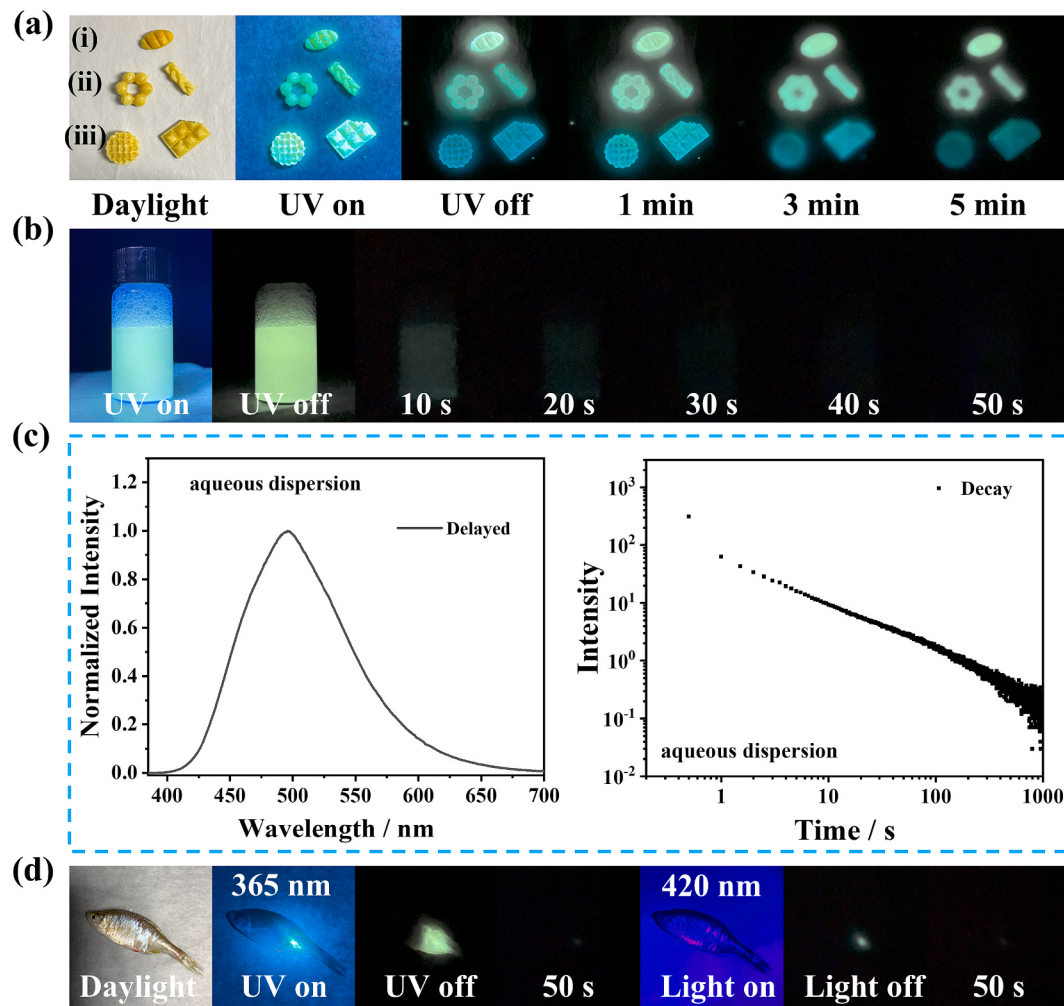


**Fig. 5.** (a) Photographs of different shapes OLPL materials of (i) NapMeOB<sub>2</sub>-MeOPhB-TMB-0.5 %, (ii) BrMeOB<sub>2</sub>-MeOPhB-TMB-0.3 % and (iii) DPMeOB<sub>2</sub>-MeOPhB-TMB-0.3 % under 365 nm UV light excitation and after the removal of the UV light. (b) Photographs of NapMeOB<sub>2</sub>-MeOPhB-TMB-0.5 % aqueous dispersion under 365 nm UV light excitation and after the removal of the UV light. (c) Room-temperature delayed emission spectrum and decay profile (monitored at 496 nm) of NapMeOB<sub>2</sub>-MeOPhB-TMB-0.5 % aqueous dispersion. (d) Photographs of living fish injected NapMeOB<sub>2</sub>-MeOPhB-TMB-0.5 % suspension under daylight, 365 nm UV light / 420 nm visible light and after turning off the lamp.

through melt-casting, making them suitable for display applications (Fig. 5a). Furthermore, long-lived aqueous afterglow systems hold promising potential for bioimaging. However, significant obstacles, such as oxygen quenching, render the development of prolonged aqueous afterglow materials particularly challenging. To achieve water-dispersible  $\text{BF}_2\text{bdk}$ -MeOPhB-TMB-0.5 %, the molten material was dropwise into a Pluronic F-127 surfactant aqueous solution under ultrasonic conditions (40 kHz, 180 W) at 80 °C. Polarized optical microscopy analysis revealed the presence of block-shaped crystalline microcrystals in NapMeOBF<sub>2</sub>-MeOPhB-TMB-0.5 % aqueous afterglow dispersion, exhibiting dimensions of 5–30 μm in length and 2–5 μm in width (Fig. S52). We also investigated the stability of the NapMeOBF<sub>2</sub>-MeOPhB-TMB-0.5 % afterglow suspension over time. Initial observations revealed progressive particle deposition after 1–2 h of quiescent standing (Fig. S53a). Complete deposition occurred within 17 h. The NapMeOBF<sub>2</sub>-MeOPhB-TMB-0.5 % aqueous dispersion was completely deposited after 17 h. Notably, redispersion through manual shaking restored the original colloidal state, with subsequent same deposition rate as the initial behavior (Fig. S53b). This reversible deposition-redispersion cycle persisted through multiple iterations (Fig. S53c), indicating the formed microparticles remain almost the same with good stability. The resulting homogeneous and stable aqueous dispersion retained its afterglow properties under ambient conditions, with a duration of 50 s (Fig. 5b). The delayed emission spectrum of the NapMeOBF<sub>2</sub>-MeOPhB-TMB-0.5 % aqueous dispersion displays almost identical peak with their solid state. Their delayed emission decay profile also fits the power law decay, suggesting the aqueous dispersion remain OLPL emission (Fig. 5c). Furthermore, preliminary bioimaging investigations were conducted on the NapMeOBF<sub>2</sub>-MeOPhB-TMB-0.5 % afterglow aqueous dispersion. To evaluate biocompatibility for potential biomedical applications, the cytotoxicity measurement of NapMeOBF<sub>2</sub>-MeOPhB-TMB-0.5 % aqueous dispersion was performed. The liquid extract of the aqueous dispersion maintains relative cell viability between 72 % and 92 % (Fig. S54). Upon injection of the dispersion into the living fish, a distinct green afterglow was detectable against an exceptionally clear background following exposure to either UV or visible light (Fig. 5d). These findings highlight the potential of this system for bioimaging applications.

## 7. Conclusions

In conclusion, we have successfully developed a three-component OLPL systems,  $\text{BF}_2\text{bdk}$ -MeOPhB-TMB-0.5 %, by doping  $\text{BF}_2\text{bdk}$  molecules into a MeOPhB matrix and incorporating TMB as electron donor and hole trap. These materials exhibit an intense and hour-long afterglow. By screening a series of PhB derivatives, MeOPhB was identified as the optimal matrix due to its excellent capability to disperse luminescent dopants. Further tuning of the system's OLPL performance was achieved by adjusting the doping concentration, which was optimized at 0.5 wt%. The addition of TMB effectively stabilizes the charge-separated states and mitigates quenching in the charge-separated state, enabling the material to maintain high-performance afterglow under ambient conditions. The system achieves intense afterglow with a duration exceeding 2.5 h, comparable to that of inorganic long-persistence phosphors. This strategy offers a versatile framework for extending OLPL design principles to other material systems, significantly expanding the range of afterglow materials. Notably, the aqueous dispersion of this three-component system retains its robust OLPL characteristics, suggesting promising applications in bioimaging and other advanced fields.

## CRediT authorship contribution statement

**Biao Xu:** Writing – original draft, Validation, Software, Data curation, Conceptualization. **Guangming Wang:** Software, Data curation. **Hongxin Gao:** Software, Data curation. **Tengyue Wang:** Visualization,

Validation. **Zi Ye:** Validation. **Wen Xia:** Validation. **Qianhui Chong:** Validation. **Qianqian Yan:** Writing – original draft, Visualization, Data curation. **Kaka Zhang:** Writing – review & editing, Supervision, Funding acquisition, Conceptualization.

## Declaration of competing interest

The authors declare that they have no known competing financial interests or personal relationships that could have appeared to influence the work reported in this paper.

## Acknowledgments

We thank the financial supports from National Natural Science Foundation of China (22475228, 22175194), the Strategic Priority Research Program of the Chinese Academy of Sciences (XDB06100000), Hundred Talents Program from Shanghai Institute of Organic Chemistry (Y121078), Pioneer Hundred Talents Program of Chinese Academy of Sciences (E320021), and Ningbo Natural Science Foundation (2023J243).

## Appendix A. Supplementary data

Supplementary data to this article can be found online at <https://doi.org/10.1016/j.cej.2025.163359>.

## Data availability

Data will be made available on request.

## References

- [1] V.-W.-W. Yam, V.-K.-M. Au, S.-Y.-L. Leung, Light-emitting self-assembled materials based on  $d^8$  and  $d^{10}$  transition metal complexes, *Chem. Rev.* 115 (2015) 7589–7728, <https://doi.org/10.1021/acs.chemrev.5b00074>.
- [2] R. Kabe, C. Adachi, Organic long persistent luminescence, *Nature* 550 (2017) 384–387, <https://doi.org/10.1038/nature24010>.
- [3] W. Zhao, Z. He, B.Z. Tang, Room-temperature phosphorescence from organic aggregates, *Nat. Rev. Mater.* 5 (2020) 869–885, <https://doi.org/10.1038/s41578-020-0223-z>.
- [4] N. Gan, H. Shi, Z. An, W. Huang, Recent advances in polymer-based metal-free room-temperature phosphorescent materials, *Adv. Funct. Mater.* 28 (2018) 1802657, <https://doi.org/10.1002/adfm.201802657>.
- [5] S. Hirata, Recent advances in materials with room-temperature phosphorescence: photophysics for triplet exciton stabilization, *Adv. Opt. Mater.* 5 (2017) 1700116, <https://doi.org/10.1002/adom.201700116>.
- [6] C. Kenry, B. Chen, Liu, Enhancing the performance of pure organic room-temperature phosphorescent luminophores, *Nat. Commun.* 10 (2019) 2111, <https://doi.org/10.1038/s41467-019-10033-2>.
- [7] X. Ma, J. Wang, H. Tian, Assembling-induced emission: an efficient approach for amorphous metal-free organic emitting materials with room-temperature phosphorescence, *Acc. Chem. Res.* 52 (2019) 738–748, <https://doi.org/10.1021/acs.accounts.8b00620>.
- [8] X. Yang, G.I.N. Waterhouse, S. Lu, J. Yu, Recent advances in the design of afterglow materials: mechanisms, structural regulation strategies and applications, *Chem. Soc. Rev.* 52 (2023) 8005–8058, <https://doi.org/10.1039/DCSR00993E>.
- [9] K. Jinna, R. Kabe, C. Adachi, Wide-range tuning and enhancement of organic long-persistent luminescence using emitter dopants, *Adv. Mater.* 30 (2018) 1800365, <https://doi.org/10.1002/adma.201800365>.
- [10] K. Jinna, N. Nishimura, R. Kabe, C. Adachi, Fabrication-method independence of organic long-persistent luminescence performance, *Chem. Lett.* 48 (2019) 270–273, <https://doi.org/10.1246/cl.180949>.
- [11] J. Yang, Z. Chen, M. Fang, Z. Li, Recent advances of organic long persistent luminescence: Design strategy and internal mechanism, *Smart Mol.* 2 (2024) e20240034, <https://doi.org/10.1002/sm.20240034>.
- [12] K. Jinna, R. Kabe, Z. Lin, C. Adachi, Organic long-persistent luminescence stimulated by visible light in p-type systems based on organic photoredox catalyst dopants, *Nat. Mater.* 21 (2022) 338–344, <https://doi.org/10.1038/s41563-021-01150-9>.
- [13] G. Wang, X. Chen, Y. Zeng, X. Li, X. Wang, K. Zhang, Dual-mechanism design strategy for high-efficiency and long-lived organic afterglow materials, *J. Am. Chem. Soc.* 146 (2024) 24871–24883, <https://doi.org/10.1021/jacs.4c05531>.
- [14] R. Gao, M.S. Kodaimati, D. Yan, Recent advances in persistent luminescence based on molecular hybrid materials, *Chem. Soc. Rev.* 50 (2021) 5564–5589, <https://doi.org/10.1039/D0CS01463J>.

- [15] Y. Wang, H. Gao, J. Yang, M. Fang, D. Ding, B.Z. Tang, Z. Li, High performance of simple organic phosphorescence host–guest materials and their application in time-resolved bioimaging, *Adv. Mater.* 33 (2021) 2007811, <https://doi.org/10.1002/adma.202007811>.
- [16] Z. Lin, R. Kabe, N. Nishimura, K. Jinnai, C. Adachi, Organic long-persistent luminescence from a flexible and transparent doped polymer, *Adv. Mater.* 30 (2018) 1803713, <https://doi.org/10.1002/adma.201803713>.
- [17] G. Wang, X. Chen, X. Li, Y. Zeng, K. Zhang, Mechanism landscape in pyrylium induced organic afterglow systems, *Chem. Sci.* 14 (2023) 8180–8186, <https://doi.org/10.1039/DSC01500A>.
- [18] H. Ohkita, W. Sakai, A. Tsuchida, M. Yamamoto, Charge recombination of electron–cation pairs formed in polymer solids at 20 K through two-photon ionization, *J. Phys. Chem. B* 101 (1997) 10241–10247, <https://doi.org/10.1021/jp971897y>.
- [19] W. Li, Z. Li, C. Si, M.Y. Wong, K. Jinnai, A.K. Gupta, R. Kabe, C. Adachi, W. Huang, E. Zysman-Colman, I.D.W. Samuel, Organic long-persistent luminescence from a thermally activated delayed fluorescence compound, *Adv. Mater.* 32 (2020) 2003911, <https://doi.org/10.1002/adma.202003911>.
- [20] X. Liang, Y. Zheng, J. Zuo, Two-photon ionization induced stable white organic long persistent luminescence, *Angew. Chem. Int. Ed.* 60 (2021) 16984–16988, <https://doi.org/10.1002/anie.202106472>.
- [21] P. Alam, T.S. Cheung, N.L.C. Leung, J. Zhang, J. Guo, L. Du, R.T.K. Kwok, J.W. Y. Lam, Z. Zeng, D.L. Phillips, H.H.Y. Sung, I.D. Williams, B.Z. Tang, Organic long-persistent luminescence from a single-component aggregate, *J. Am. Chem. Soc.* 144 (2022) 3050–3062, <https://doi.org/10.1021/jacs.1c11480>.
- [22] C. Lin, Z. Wu, H. Ma, J. Liu, S. You, A. Lv, W. Ye, J. Xu, H. Shi, B. Zha, W. Huang, Z. An, Y. Zhuang, R.-J. Xie, Charge trapping for controllable persistent luminescence in organics, *Nat. Photonics* 18 (2024) 350–356, <https://doi.org/10.1038/s41566-024-01396-0>.
- [23] P. Jin, X. Wei, B. Yin, L. Xu, Y. Guo, C. Zhang, Stepwise charge/energy transfer in MR-TADF molecule-doped exciplex for ultralong persistent luminescence activated with visible light, *Adv. Mater.* 36 (2024) 2400158, <https://doi.org/10.1002/adma.202400158>.
- [24] G. Xie, M. Zeng, X. Zhang, A. Luo, J. Zhang, F. He, X. Wang, Y. Hu, W. Wang, Y. Xie, H. Li, R. Chen, Y. Tao, Developing stable organic radical anions to achieve long persistent luminescence for afterglow lighting, *Sci. China Mater.* 66 (2023) 4756–4763, <https://doi.org/10.1007/s40843-023-2590-x>.
- [25] Z. Lin, R. Kabe, K. Wang, C. Adachi, Influence of energy gap between charge-transfer and locally excited states on organic long persistence luminescence, *Nat. Commun.* 11 (2020) 191, <https://doi.org/10.1038/s41467-019-14035-y>.
- [26] Y. Zhao, B. Ding, Z. Huang, X. Ma, Highly efficient organic long persistent luminescence based on host–guest doping systems, *Chem. Sci.* 13 (2022) 8412–8416, <https://doi.org/10.1039/DSC01622B>.
- [27] Y. Zhou, P. Zhang, Z. Liu, W. Yan, H. Gao, G. Liang, W. Qin, Sunlight-activated hour-long afterglow from transparent and flexible polymers, *Adv. Mater.* 36 (2024) 2312439, <https://doi.org/10.1002/adma.202312439>.
- [28] W.Z. Yuan, X.Y. Shen, H. Zhao, J.W.Y. Lam, L. Tang, P. Lu, C. Wang, Y. Liu, Z. Wang, Q. Zheng, J.Z. Sun, Y. Ma, B.Z. Tang, Crystallization-induced phosphorescence of pure organic luminogens at room temperature, *J. Phys. Chem. C* 114 (2010) 6090–6099, <https://doi.org/10.1021/jp09388y>.
- [29] G. Yin, J. Zhou, W. Lu, L. Li, D. Liu, M. Qi, B.Z. Tang, P. Théato, T. Chen, Targeting compact and ordered emitters by supramolecular dynamic interactions for high-performance organic ambient phosphorescence, *Adv. Mater.* 36 (2024) 2311347, <https://doi.org/10.1002/adma.202311347>.
- [30] D. Li, F. Lu, J. Wang, W. Hu, X.-M. Cao, X. Ma, H. Tian, Amorphous metal-free room-temperature phosphorescent small molecules with multicolor photoluminescence via a host–guest and dual-emission strategy, *J. Am. Chem. Soc.* 140 (2018) 1916–1923, <https://doi.org/10.1021/jacs.7b12800>.
- [31] X. Zhen, Y. Tao, Z. An, P. Chen, C. Xu, R. Chen, W. Huang, K. Pu, Ultralong phosphorescence of water-soluble organic nanoparticles for in vivo afterglow imaging, *Adv. Mater.* 29 (2017) 1606665, <https://doi.org/10.1002/adma.201606665>.
- [32] X.-K. Ma, Y. Liu, Supramolecular purely organic room-temperature phosphorescence, *Acc. Chem. Res.* 54 (2021) 3403–3414, <https://doi.org/10.1021/acs.accounts.1c00336>.
- [33] J.-X. Wang, H. Zhang, L.-Y. Niu, X. Zhu, Y.-F. Kang, R. Boulatov, Q.-Z. Yang, Organic composite crystal with persistent room-temperature luminescence above 650 nm by combining triplet–triplet energy transfer with thermally activated delayed fluorescence, *CCS Chem.* 2 (2020) 1391–1398, <https://doi.org/10.31635/ccschem.020.202000158>.
- [34] J. You, X. Zhang, Q. Nan, K. Jin, J. Zhang, Y. Wang, C. Yin, Z. Yang, J. Zhang, Aggregation-regulated room-temperature phosphorescence materials with multi-mode emission, adjustable excitation-dependence and visible-light excitation, *Nat. Commun.* 14 (2023) 4163, <https://doi.org/10.1038/s41467-023-39767-w>.
- [35] S.M.A. Fateminia, Z. Mao, S. Xu, Z. Yang, Z. Chi, B. Liu, Organic nanocrystals with bright red persistent room-temperature phosphorescence for biological applications, *Angew. Chem. Int. Ed.* 56 (2017) 12160–12164, <https://doi.org/10.1002/anie.201705945>.
- [36] Y. Zhang, Y. Su, H. Wu, Z. Wang, C. Wang, Y. Zheng, X. Zheng, L. Gao, Q. Zhou, Y. Yang, X. Chen, C. Yang, Y. Zhao, Large-area, flexible, transparent, and long-lived polymer-based phosphorescence films, *J. Am. Chem. Soc.* 143 (2021) 13675–13685, <https://doi.org/10.1021/jacs.1c05213>.
- [37] S. Hirata, K. Totani, J. Zhang, T. Yamashita, H. Kaji, S.R. Marder, T. Watanabe, C. Adachi, Efficient persistent room temperature phosphorescence in organic amorphous materials under ambient conditions, *Adv. Funct. Mater.* 23 (2013) 3386–3397, <https://doi.org/10.1002/adfm.201203706>.
- [38] Q. Zhang, S. Wang, X. Xiong, P. Fu, X. Zhang, Y. Fan, M. Pan, High-temperature and dynamic RGB (red-green-blue) long-persistent luminescence in an anti-kasha organic compound, *Angew. Chem. Int. Ed.* 61 (2022) e202205556, <https://doi.org/10.1002/anie.202205556>.
- [39] Y. Liang, P. Hu, H. Zhang, Q. Yang, H. Wei, R. Chen, J. Yu, C. Liu, Y. Wang, S. Luo, G. Shi, Z. Chi, B. Xu, Enabling highly robust full-color ultralong room-temperature phosphorescence and stable white organic afterglow from polycyclic aromatic hydrocarbons, *Angew. Chem. Int. Ed.* 63 (2024) e202318516, <https://doi.org/10.1002/anie.202318516>.
- [40] X. Yan, H. Peng, Y. Xiang, J. Wang, L. Yu, Y. Tao, H. Li, W. Huang, R. Chen, Recent advances on host–guest material systems toward organic room temperature phosphorescence, *Small* 18 (2022) 2104073, <https://doi.org/10.1002/smll.202104073>.
- [41] H. Gao, X. Ma, Recent progress on pure organic room temperature phosphorescent polymers, *Aggregate* 2 (2021) e38.
- [42] L. Ma, X. Ma, Recent advances in room-temperature phosphorescent materials by manipulating intermolecular interactions, *Sci. China Chem.* 66 (2023) 304–314, <https://doi.org/10.1007/s11426-022-1400-6>.
- [43] X. Zhang, M. Zeng, Y. Zhang, C. Zhang, Z. Gao, F. He, X. Xue, H. Li, P. Li, G. Xie, H. Li, X. Zhang, N. Guo, H. Cheng, A. Luo, W. Zhao, Y. Zhang, Y. Tao, R. Chen, W. Huang, Multicolor hyperafterglow from isolated fluorescence chromophores, *Nat. Commun.* 14 (2023) 475, <https://doi.org/10.1038/s41467-023-36105-y>.
- [44] Y. Lei, W. Dai, J. Guan, S. Guo, F. Ren, Y. Zhou, J. Shi, B. Tong, Z. Cai, J. Zheng, Y. Dong, Wide-range color-tunable organic phosphorescence materials for printable and writable security inks, *Angew. Chem. Int. Ed.* 59 (2020) 16054–16060, <https://doi.org/10.1002/anie.202003585>.
- [45] Z. Yang, C. Xu, W. Li, Z. Mao, X. Ge, Q. Huang, H. Deng, J. Zhao, F.L. Gu, Y. Zhang, Z. Chi, Boosting the quantum efficiency of ultralong organic phosphorescence up to 52 % via intramolecular halogen bonding, *Angew. Chem. Int. Ed.* 59 (2020) 17451–17455, <https://doi.org/10.1002/anie.202007343>.
- [46] Z. Xu, Y. He, H. Shi, Z. An, Room-temperature phosphorescence materials from crystalline to amorphous state, *SmartMat* 4 (2023) e1139.
- [47] N. Xue, H.-Y. Zhou, Y. Han, M. Li, H.-Y. Lu, C.-F. Chen, A general supramolecular strategy for fabricating full-color-tunable thermally activated delayed fluorescence materials, *Nat. Commun.* 15 (2024) 1425, <https://doi.org/10.1038/s41467-024-45717-x>.
- [48] J. Yang, X. Zhen, B. Wang, X. Gao, Z. Ren, J. Wang, Y. Xie, J. Li, Q. Peng, K. Pu, Z. Li, The influence of the molecular packing on the room temperature phosphorescence of purely organic luminogens, *Nat. Commun.* 9 (2018) 840, <https://doi.org/10.1038/s41467-018-03236-6>.
- [49] Q. Yan, J. Li, T. Wang, W. Xia, G. Wang, H. Li, K. Zhang, Aqueous-phase room-temperature afterglow crystalline micro/nanostructures via supramolecular inclusion complexation of γ-cyclodextrin with difluoroboron β-diketonate luminescence compounds, *Next Mater.* 7 (2025) 100379, <https://doi.org/10.1016/j.nxmate.2024.100379>.
- [50] X. Wang, Y. Sun, G. Wang, J. Li, X. Li, K. Zhang, TADF-type organic afterglow, *Angew. Chem. Int. Ed.* 60 (2021) 17138–17147, <https://doi.org/10.1002/anie.202105628>.
- [51] Y. Sun, G. Wang, X. Li, B. Zhou, K. Zhang, Achieving high afterglow brightness in organic dopant-matrix systems, *Adv. Opt. Mater.* 9 (2021) 2100353, <https://doi.org/10.1002/adom.202100353>.
- [52] J. Li, G. Wang, X. Chen, X. Li, M. Wu, S. Yuan, Y. Zou, X. Wang, K. Zhang, Manipulation of triplet excited states in two-component systems for high-performance organic afterglow materials, *Chem. – Eur. J.* 28 (2022) e202200852, <https://doi.org/10.1002/chem.202200852>.
- [53] J. Li, X. Li, G. Wang, X. Wang, M. Wu, J. Liu, K. Zhang, A direct observation of up-converted room-temperature phosphorescence in an anti-Kasha dopant-matrix system, *Nat. Commun.* 14 (2023) 1987, <https://doi.org/10.1038/s41467-023-37662-y>.
- [54] B. Zhou, D. Yan, Hydrogen-bonded two-component ionic crystals showing enhanced long-lived room-temperature phosphorescence via TADF-assisted Förster resonance energy transfer, *Adv. Funct. Mater.* 29 (2019) 1807599, <https://doi.org/10.1002/adfm.201807599>.
- [55] D. Yan, D.G. Evans, Molecular crystalline materials with tunable luminescent properties: from polymers to multi-component solids, *Mater. Horiz.* 1 (2014) 46–57, <https://doi.org/10.1039/C3MH00023K>.
- [56] P.-Z. Chen, L.-Y. Niu, Y.-Z. Chen, Q.-Z. Yang, Difluoroboron β-diketonate dyes: Spectroscopic properties and applications, *Coord. Chem. Rev.* 350 (2017) 196–216, <https://doi.org/10.1016/j.ccr.2017.06.026>.
- [57] G. Zhang, G.M. Palmer, M.W. Dewhurst, C.L. Fraser, A dual-emissive-materials design concept enables tumour hypoxia imaging, *Nat. Mater.* 8 (2009) 747–751, <https://doi.org/10.1038/nmat2509>.
- [58] X.-F. Wang, H. Xiao, P.-Z. Chen, Q.-Z. Yang, B. Chen, C.-H. Tung, Y.-Z. Chen, L.-Z. Wu, Pure organic room temperature phosphorescence from excited dimers in self-assembled nanoparticles under visible and near-infrared irradiation in water, *J. Am. Chem. Soc.* 141 (2019) 5045–5050, <https://doi.org/10.1021/jacs.9b00859>.
- [59] T. Wang, X. Wang, Q. Yan, K. Zhang, Ultralong organic room-temperature phosphorescence modulated by balancing intramolecular charge transfer and localized excitation character of excited states, *Dyes Pigm.* 224 (2024) 112024, <https://doi.org/10.1016/j.dyepig.2024.112024>.
- [60] Y. Sun, J. Liu, J. Li, X. Li, X. Wang, G. Wang, K. Zhang, Manipulation of triplet excited states for long-lived and efficient organic afterglow, *Adv. Opt. Mater.* 10 (2022) 2101909, <https://doi.org/10.1002/adom.202101909>.
- [61] D.-H. Kim, A. D'Aleó, X.-K. Chen, A.D.S. Sandanayaka, D. Yao, L. Zhao, T. Komino, E. Zaborova, G. Canard, Y. Tsuchiya, E. Choi, J.W. Wu, F. Fages, J.-L. Brédas, J.-C. Ribierre, C. Adachi, High-efficiency electroluminescence and amplified

- spontaneous emission from a thermally activated delayed fluorescent near-infrared emitter, *Nat. Photonics* 12 (2018) 98–104, <https://doi.org/10.1038/s41566-017-0087-y>.
- [62] N.R. Paisley, S.V. Halldorson, M.V. Tran, R. Gupta, S. Kamal, W.R. Algar, Z. M. Hudson, Near-infrared-emitting boron-difluoride-curcuminoid-based polymers exhibiting thermally activated delayed fluorescence as biological imaging probes, *Angew. Chem. Int. Ed.* 60 (2021) 18630–18638, <https://doi.org/10.1002/anie.202103965>.
- [63] W.H. Hamill, Debye–Edwards electron recombination kinetics, *J. Chem. Phys.* 71 (1979) 140–142, <https://doi.org/10.1063/1.438113>.
- [64] S. Kuila, S.J. George, Phosphorescence energy transfer: ambient afterglow fluorescence from water-processable and purely organic dyes via delayed sensitization, *Angew. Chem. Int. Ed.* 59 (2020) 9393–9397, <https://doi.org/10.1002/anie.202002555>.
- [65] S. Xu, W. Wang, H. Li, J. Zhang, R. Chen, S. Wang, C. Zheng, G. Xing, C. Song, W. Huang, Design of highly efficient deep-blue organic afterglow through guest sensitization and matrices rigidification, *Nat. Commun.* 11 (2020) 4802, <https://doi.org/10.1038/s41467-020-18572-9>.
- [66] M. Sakurai, R. Kabe, M. Fukui, Z. Lin, K. Jinnai, Y. Kobori, C. Adachi, T. Tachikawa, Organic photostimulated luminescence associated with persistent spin-correlated radical pairs, *Commun. Mater.* 2 (2021) 74, <https://doi.org/10.1038/s43246-021-00178-3>.
- [67] R. Arce, L. Kevan, Photochemical behaviour of N,N,N',N'-tetramethylbenzidine and its protonated forms in sodium dodecyl sulphate anionic micelles under 337 nm laser irradiation, *J. Chem. Soc. Faraday Trans. 1* (81) (1985) 1669–1676, <https://doi.org/10.1039/F19858101669>.
- [68] Y. Sasaki, Y. Yoshikawa, A. Watanabe, O. Ito, Solvent effect on photoinduced electron transfer between C<sub>60</sub> and 3,3',5,5'-tetramethylbenzidine studied by nanosecond laser photolysis, *J. Chem. Soc. Faraday Trans. 91* (1995) 2287–2290, <https://doi.org/10.1039/FT9959102287>.
- [69] K. Kiruthiga, P. Aravindan, S. Anandan, P. Maruthamuthu, Investigation on the formation and decay of the N,N,N',N'-tetramethylbenzidine radical cation using various oxidants and reductants by stopped-flow spectrophotometry, *Res. Chem. Intermed.* 32 (2006) 115–135, <https://doi.org/10.1163/156856706775372807>.
- [70] H. Gao, G. Wang, T. Wang, Z. Ye, Q. Yan, Q. Chong, C. Chan, B. Wang, K. Zhang, Achieving high-performance organic long persistent luminescence materials via manipulation of radical cation stability, *Adv. Sci.* 12 (2025) 2416853, <https://doi.org/10.1002/advs.202416853>.